Chong *et al. Bioresour. Bioprocess.* (2019) 6:21
https://doi.org/10.1186/s40643-019-0254-8

Bioresources and Bioprocessing

RESEARCH Open Access

Characterization of a recombinant thermotolerant argonaute protein as an endonuclease by broad guide utilization

Yuesheng Chong, Qian Liu, Fei Huang, Dong Song and Yan Feng*

Abstract

Background: Prokaryotic argonaute proteins (pAgos) play an important role in host defense in vivo. Most importantly, the thermophilic pAgos with endonuclease activity hold great potential for programmable genetic manipulation. Therefore, exploring argonaute proteins with unique enzyme properties is desired for understanding their diverse catalytic mechanisms and promoting their applications in biotechnology.

Results: The argonaute protein from archaeon *Methanocaldococcus fervens* (*Mf*Ago) was cloned and overexpressed in *Escherichia coli* BL21 (DE3). The recombinant protein showed the expected molecular weight of ~ 85.8 kDa by SDS-PAGE. The activity assays demonstrate that *Mf*Ago has cleavage activities toward single-stranded DNA (ssDNA) targets specifically at the site complementary to the position between nucleotides 10 and 11 of the guide strand. Interestingly, *Mf*Ago utilizes small 5′-phosphorylated ssDNA (5′-P ssDNA), 5′-hydroxylated ssDNA (5′-OH ssDNA), and 5′-phosphorylated ssRNA (5′-P ssRNA) as the guides for catalysis. The optimal temperatures are highly dependent on the type of guide and have a range of 80–90 °C. The addition of 0.5 mM Mn^{2+}, Mg^{2+} or Co^{2+} to the reaction system significantly enhanced the enzyme activity. Meanwhile, *Mf*Ago is quite active at NaCl concentrations less than 500 mM. Furthermore, structural modeling analyses suggested that its unique wide guide-dependent activity might be related to differing multiple interactions between guides and the MID domain of *Mf*Ago.

Conclusions: *Mf*Ago shows efficient endonuclease activity for ssDNA cleavage. In contrast to most known pAgos, which recognize only one type of guide, *Mf*Ago uses diverse guides, including 5′-P ssDNA, 5′-OH ssDNA, and 5′-P ssRNA, to specifically cleave targets. Characterization of *Mf*Ago expands the understanding of catalysis in the Ago family and provides clues for future genetic manipulation.

Keywords: Argonaute protein, Nucleic acid guide, Endonuclease, DNA cleavage, Homologous modeling

Background

Argonaute proteins (Agos) are widely present in all domains of life and bind small DNA or RNA guides to specifically recognize—and sometimes cleave—complementary nucleic acid targets (Swarts et al. 2014a). Eukaryotic argonaute proteins (eAgos) are the key components in RNA interference (RNAi) pathways that participate in the regulation of post-transcriptional gene expression (Bartel 2009; Ketting 2011; Meister 2013; Siomi et al. 2011). Recently, pAgos, including bacterial and archaeal Agos, were supposed to participate in host defense processes by interfering with exogenous nucleic acid infection (Olovnikov et al. 2013; Swarts et al. 2014a, 2015a, b). Genome analysis of prokaryotes reveals that pAgos are more diverse than eAgos since they are distributed in ~ 30% of bacterial and ~ 10% of archaeal sequenced genomes (Koonin 2017; Makarova et al. 2009; Swarts et al. 2014b). The functions of pAgos are relatively poorly understood and need to be further investigated.

Previous structural and biochemical studies of pAgos from thermophilic prokaryotes showed that they exhibit

*Correspondence: yfeng2009@sjtu.edu.cn
State Key Laboratory of Microbial Metabolism, School of Life Sciences and Biotechnology, Shanghai Jiao Tong University, 800 Dongchuan Road, Shanghai 200240, China

endonuclease activity directed by nucleic acid guides, which is similar to CRISPR–Cas9 activity. The characterized pAgos showed a preference for high temperature, generally ranging from 65 to 95 °C, and a divalent cation requirement. As an endonuclease of Watson–Crick guide-target pairing, the pAgos have unique guide preferences. To date, most pAgos perform specific cleavage via one type of guide from all four natural types of small nucleic acids: 5′-P ssDNA, 5′-OH ssDNA, 5′-OH ssRNA, and 5′-P ssRNA. For example, Agos from *Pyrococcus furiosus* (*Pf*Ago) (Rivas et al. 2005; Song et al. 2004; Swarts et al. 2015a), *Aquifex aeolicus* (*Aa*Ago) (Rashid et al. 2007; Yuan et al. 2005, 2006), *Methanocaldococcus jannaschii* (*Mj*Ago) (Willkomm et al. 2017; Zander et al. 2014, 2017), and *Thermus thermophilus* (*Tt*Ago) (Sheng et al. 2014; Swarts et al. 2014a, 2015b, 2017; Wang et al. 2008a, b, 2009) cleave complementary nucleic acid targets using 5′-P ssDNA guides. Meanwhile, Agos from *Marinitoga piezophila* (*Mp*Ago) (Doxzen and Doudna 2017; Kaya et al. 2016) and *Thermotoga profunda* (*Tp*Ago) (Kaya et al. 2016) use the 5′-OH ssRNA guide to cleave nucleic acid targets, whereas the *Rhodobacter sphaeroides* Ago (*Rs*Ago) (Miyoshi et al. 2016; Olovnikov et al. 2013) utilizes a 5′-P ssRNA guide to recognize cognate nucleic acid targets (Table 1). Notably, the structural analysis indicates that the distinct guide preferences are strongly associated with the guide 5′-end-binding pocket of the MID domain, as reasoned by the available space and hydrophobic or charged environment (Kaya et al. 2016; Wang et al. 2008b).

Recently, the application of Agos has gradually attracted researchers' interest. Based on *Pf*Ago-specific dsDNA cleavage via a pair of 5′-P ssDNA guides, the artificial restriction enzymes' (AREs) platform has been developed to enable to cleave target DNA sequences at virtually any arbitrary site (Enghiad and Zhao 2017). Further, mining and biochemical characterizations of pAgos are greatly demanded to understand their basic biological roles and to explore their application potentials for genome manipulation (Ryazansky et al. 2018).

Based on a phylogenetic tree analysis, we found a putative endonuclease pAgo from the hyperthermophilic archaeon *Methanocaldococcus fervens* (*Mf*Ago). To better understand its catalytic function, *MfAgo* was cloned and overexpressed in *E. coli* BL21 (DE3) for biochemical characterization. Moreover, computational simulation analysis was carried out to reveal its nucleic acid guide preferences. Our study demonstrates that *MfAgo* is a unique endonuclease with DNA cleavage activity directed by a wide range of guides that provides a new enzyme resource for future gene manipulation.

Methods

Bacterial strain, plasmid, and medium

The host strain *E. coli* BL21(DE3) was purchased from Novagen (Madison, WI). The recombinant plasmid pET-28a(+)-*Mf*Ago, containing the synthesized codon-optimized *Mf*Ago gene, was constructed (Genscript, China). Luria–Bertani (LB) medium (tryptone 10 g/L, yeast extract 5 g/L, NaCl 10 g/L) was used for *Mf*Ago expression.

Phylogenetic tree and sequence alignment

A similarity search for the *Pf*Ago amino acid sequence was performed by BLAST in the NCBI database, and

Table 1 Guide and target preferences of characterized pAgo proteins

pAgo proteins		Guide information		Activity				References
Host	Argonaute name	Guide	5′-end nucleotide preference	RNA-guided RNA interference	RNA-guided DNA interference	DNA-guided RNA interference	DNA-guided DNA interference	
Methanocaldococcus jannaschii	*Mj*Ago	DNA	5′-P	–	–	–	+	Zander et al. (2014)
Rhodobacter sphaeroides	*Rs*Ago	RNA	5′-P	–	+	–	–	Olovnikov et al. (2013)
Aquifex aeolicus	*Aa*Ago	DNA	5′-P	–	–	+	–	Yuan et al. (2005)
Marinitoga piezophila	*Mp*Ago	RNA	5′-OH	+	+	–	–	Kaya et al. (2016)
Thermotoga profunda	*Tp*Ago	RNA	5′-OH	–	+	–	–	Kaya et al. (2016)
Thermus thermophilus	*Tt*Ago	DNA	5′-P	–	–	+	+	Wang et al. (2008a)
Pyrococcus furiosus	*Pf*Ago	DNA	5′-P	–	–	–	+	Swarts et al. (2015a)

Ago sequences with high sequence identity were selected and analyzed by MEGA 7.0 software (Kumar et al. 2016) to construct a phylogenetic tree. The sequence alignments of the Ago family were carried out using ClustalW (Thompson et al. 1994). For clarity, only residues forming the active sites are displayed.

Cloning and expression of *Mf*Ago in *E. coli* BL21 (DE3)

The expression vector pET-28a(+)-*Mf*Ago was transformed into the *E. coli* BL21 (DE3) strain to express the recombinant *Mf*Ago. Then, the positive clones were propagated overnight in a shaker incubator at 37 °C and 220 rpm in 5-mL LB medium containing 100 μg/mL kanamycin. After overnight incubation, the seed culture (1%) was inoculated into 1-L LB medium containing 100 μg/mL kanamycin at 37 °C and incubated at 220 rpm until an OD_{600} value of 0.6–0.8 was reached. Cultures were cold-shocked by incubation in an ice bath for 15 min. Protein expression was then induced by the addition of isopropyl β-D-thiogalactopyranoside (IPTG) to a final concentration of 1 mM, followed by incubation for 16 h at 20 °C and 220 rpm in a shaker incubator. Cells were harvested for centrifugation for 20 min at 6000 rpm, and the cell pellet was collected for later purification.

Purification of recombinant *Mf*Ago

The harvested cell pellets were resuspended in lysis buffer (20 mM Tris–HCl, 1 M NaCl, pH 8.0) and then disrupted using a high-pressure homogenizer (Gefran, Italy) at 600–800 bar for 3 min. The lysates were incubated at 65 °C for 15 min to eliminate most of the endogenous proteins of *E. coli* BL21 (DE3). Then, the solution was centrifuged for 30 min at 4 °C and 12,000 rpm, and then, the supernatants were loaded onto an Ni–NTA column. The N-terminal His-tagged *Mf*Ago was eluted with elution buffer (20 mM Tris–HCl, 1 M NaCl, 200 mM imidazole, pH 8.0). Finally, size-exclusion chromatography (Superdex 200, GE) was further carried out with FPLC (Agilent, USA). The eluted recombinant protein was detected and analyzed by 15% SDS-PAGE. The concentration of purified *Mf*Ago was measured by the bicinchoninic acid (BCA) method (Yeasen, China), and the fractions containing the protein were frozen at − 80 °C in storage buffer (20 mM Tris–HCl, 1 M NaCl, 15% (v/v) glycerol, pH 8.0).

Enzymatic characteristics of the recombinant *Mf*Ago in vitro

Endonuclease activity assays

The ssDNA or ssRNA guides and fluorescently labeled ssDNA or ssRNA targets were synthesized commercially (Genscript, China). For activity assays, 2.5 μM purified *Mf*Ago, 2 μM ssDNA or ssRNA guide, and 1 μM fluorescently labeled ssDNA or ssRNA target were mixed in a reaction buffer (15 mM Tris–HCl, 250 mM NaCl, 0.5 mM $MnCl_2$, pH 8.0) and then incubated for 35 min at 85 °C in a thermocycler (Eppendorf, GER). After high-temperature incubation, the reactions were stopped via the addition of loading buffer (95% formamide, 0.5 mmol/L EDTA, 0.025% bromophenol blue, 0.025% xylene cyanol FF) at a 1:1 ratio (v/v). Then, the samples were resolved on 16% denaturing polyacrylamide gels. The gels were visualized on a Fuji FLA7000 scanner with fluorescence measurements with a λ_{ex} of 535 nm and a λ_{em} of 595 nm. All the nucleic acids used in this study are listed in Table 2.

MfAgo activity at the varied temperatures

The effects of temperature on *Mf*Ago activity mediated by different guides were determined at various temperatures from 55 to 99 °C. Generally, 2.5 μM *Mf*Ago, 2 μM ssDNA or ssRNA guide, and 0.8 μM ssDNA targets were mixed in the reaction buffer and then incubated for 30 min at 54.8, 58.3, 60.7, 66.0, 71.0, 75.0, 80.0, 85.0, 90.0, 95.1, 96.9, and 98.7 °C, respectively. The samples were resolved on 16% denaturing polyacrylamide gels. Gels were stained using GelRed (Biotium, USA). The nucleic acids were visualized using a G:BOX Chemi imager (Syngene, USA) and quantitatively analyzed by Quantity One (Bio-Rad, USA).

For the stability of varied guides at high temperatures, 2 μM ssDNA or ssRNA guide was first pre-incubated in the reaction buffer at 95 °C for different times: 0, 5, 10,

Table 2 Nucleic acids used in the study

Name	Sequence (5′–3′)	1st Fig.
ssDNA target (FAM)	FAM-GTCTGTGACTCCATAGAAAATCTTTCTCCTGCTCAGTGATTTCAG	Figure 3a
ssRNA target (FAM)	FAM-GUCUGUGACUCCAUAGAAAAUCUUUCUCCUGCUCAGUGAUUUCAG	Figure 3a
5′-P ssDNA guide	P-TGAAATCACTGAGCAG	Figure 3a
5′-OH ssDNA guide	HO-TGAAATCACTGAGCAG	Figure 3a
5′-P ssRNA guide	P-UGAAAUCACUGAGCAG	Figure 3a
5′-OH ssRNA guide	HO-UGAAAUCACUGAGCAG	Figure 3a
ssDNA target	GTCTGTGACTCCATAGAAAATCTTTCTCCTGCTCAGTGATTTCAGAGAGAGGATCTCGTG	Figure 4

15, and 30 min, respectively. Subsequently, with the addition of 2.5 μM *Mf*Ago and 0.8 μM ssDNA targets, the cleavage assay was performed at 80 °C for 30 min. The samples were stained and visualized as above.

Effect of divalent cations on MfAgo activity

The effects of divalent cation on *Mf*Ago cleavage activity were determined using different divalent cations. For the assays, 2.5 μM *Mf*Ago, 2 μM ssDNA or ssRNA guide, and 0.8 μM ssDNA targets were mixed in a reaction buffer (15 mM Tris–HCl, 250 mM NaCl, pH 8.0) to which different divalent cations ($FeCl_2$, $CoCl_2$, $CuCl_2$, $MgCl_2$, $MnCl_2$, $ZnCl_2$, and $CaCl_2$) were added to a final concentration of 0.5 mM, and the samples were then incubated for 30 min at 85 °C. The cleavage activity without the addition of a divalent cation was used as a control.

The optimal Mn^{2+} concentration for *Mf*Ago cleavage activity was also determined using buffer with different final concentrations of Mn^{2+}: 5, 10, 25, 50, 100, 250, 500, 1000, 2000, and 2500 μM, respectively. All the samples were stained and analyzed as above.

Effect of NaCl concentration on MfAgo activity

The influence of NaCl concentration on the catalytic activity of recombinant *Mf*Ago was investigated using buffer systems with various NaCl concentrations (50, 100, 250, 500, 750, 1000, 1500, and 2000 mM, respectively). The samples were stained and analyzed as above.

Kinetic performance of MfAgo mediated by different guides

For a cleavage kinetic analysis, the concentrations of *Mf*Ago, ssDNA targets, and different guides were the same as above. The assays were performed at 250 mM NaCl and 2 mM Mn^{2+} at 85 °C for different times: 0, 1, 3, 5, 10, 20, 30, 45, 60, 80, 100, 120, 150, and 180 min, respectively. The samples were resolved on 16% denaturing polyacrylamide gels and quantitatively analyzed by Quantity One (Bio-Rad, USA) to measure the cleavage efficiency of *Mf*Ago mediated by different guides.

Homology modeling and structural analysis

Homology modeling for *Mf*Ago was determined using the SWISS-MODEL online tool (https://www.swissmodel.expasy.org/) (Waterhouse et al. 2018) by using the binary structure of *Mj*Ago with the 5′-P ssDNA guide (PDB ID: 5G5T, identity 68%) (Willkomm et al. 2017) as the template; then, the 5′-P ssDNA, 5′-OH ssDNA, and 5′-P ssRNA guides were docked into the *Mf*Ago model structure using the Schrodinger software (Repasky et al. 2007). An electrostatic heat map and the specific region where *Mf*Ago binds the guide were analyzed by PyMol.

Results and discussion

Phylogenetic tree and sequence analysis of *Mf*Ago

To discover new functional biological resources in pAgos, we constructed a phylogenetic tree by aligning the *Pf*Ago amino acid sequences in the NCBI database (Fig. 1a). *Mf*Ago was chosen as the candidate because it is most closely related to hyperthermophilic *Mj*Ago, with 68% shared identity. Then, the sequence analysis of *Mf*Ago was performed in detail. The *Mf*Ago gene (GenBank Accession No. NC013156) was an intact open reading frame encoding the protein of 706 amino acids. Accordingly, target cleavage by all active Ago proteins is mediated by the conserved tetrad of the DEDX motif (where X can be D, H, N or K) (Kaya et al. 2016; Swarts et al. 2014b, 2015a; Yuan et al. 2005). Multiple sequence alignment was carried out, especially focusing on the regions containing the DEDX motif (Fig. 1b). Most importantly, we found that the DEDD tetrad occurred in *Mf*Ago, suggesting that *Mf*Ago may have endonuclease catalytic activity that needs characterization in vitro.

Expression and purification of the recombinant *Mf*Ago

The gene-encoding *Mf*Ago was codon-optimized and built into the plasmid pET-28a(+), which has an N-terminal His-tag and was then transformed into *E. coli* BL21(DE3). Expression in the recombinant *E. coli* BL21(DE3) was induced by IPTG at 20 °C, and the resulting protein was then purified using an Ni–NTA affinity column. SDS-PAGE analysis showed that the purified protein size was consistent with the estimated molecular weight of recombinant protein (85.8 kDa), which indicated that the recombinant *Mf*Ago was successfully expressed in *E. coli* BL21(DE3) in a soluble form (Fig. 2a). Then, the size-exclusion chromatography elution showed a single peak, indicating that the purified recombinant *Mf*Ago was a monomer (Fig. 2b). Here, the recombinant *Mf*Ago, purified by Ni–NTA and size exclusion, could be used for subsequent cleavage activity assays in vitro.

Enzymatic characterization of the recombinant *Mf*Ago in vitro

Endonuclease activity of MfAgo

To investigate the enzyme properties of the recombinant *Mf*Ago, we investigated nucleic acid cleavage via a variety of nucleic acid guides in vitro. First, we designed 16-nucleotide (nt) ssDNA or ssRNA guides with a 5′ phosphate or 5′ hydroxyl group to cleave complementary FAM-labeled ssDNA or ssRNA targets (Fig. 3a). Strikingly, the results showed that *Mf*Ago cleaved complementary ssDNA targets using 5′-P ssDNA, 5′-P ssRNA, or 5′-OH ssDNA guides (Fig. 3b). Different kinds of guide preferences have not been observed in other characterized Agos from eukaryotes or prokaryotes.

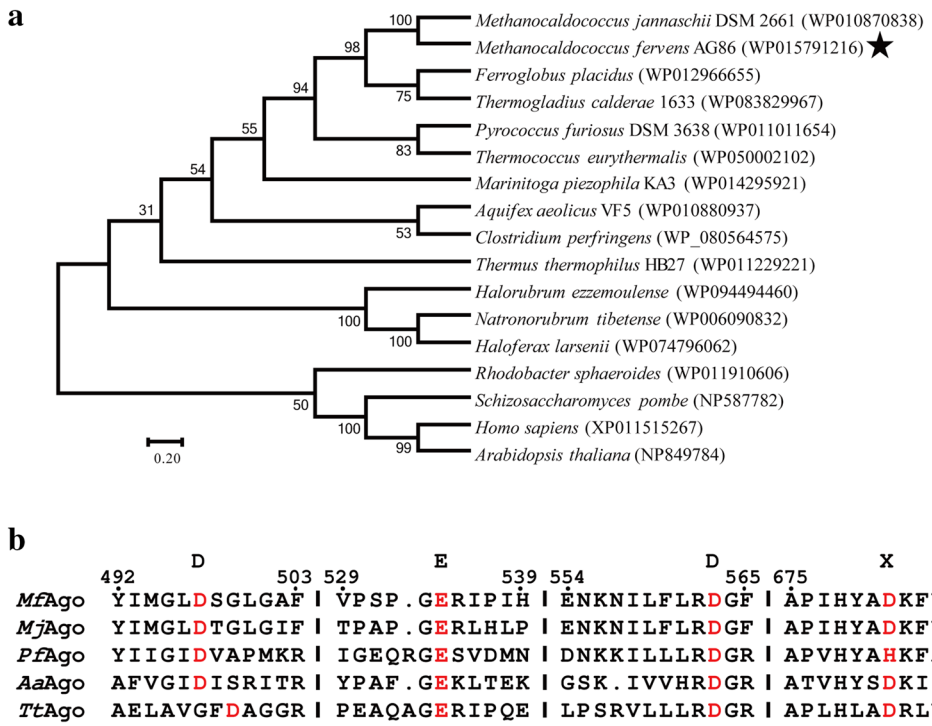

Fig. 1 Phylogenetic tree and sequence analysis. **a** Neighbor-joining phylogenetic tree analysis of *Mf*Ago based on amino acid sequences. The numbers at the nodes indicate the bootstrap values for neighbor-joining analysis of 1000 resampled data sets. The scale bar represents the evolutionary distance between species. Numbers in parentheses represent the sequence accession numbers in the NCBI database. **b** Multiple sequence alignments of *Mf*Ago with other known pAgos. *Mj*Ago: Ago from *Methanocaldococcus jannaschii*. *Pf*Ago: Ago from *Pyrococcus furiosus*. *Aa*Ago: Ago from *Aquifex aeolicus*. *Tt*Ago: Ago from *Thermus thermophilus*. Only regions containing the DEDX catalytic residues (indicated in red) are shown. The alignment was carried out using ClustalW, shaded manually and using ESPript 3.0 (Robert and Gouet 2014)

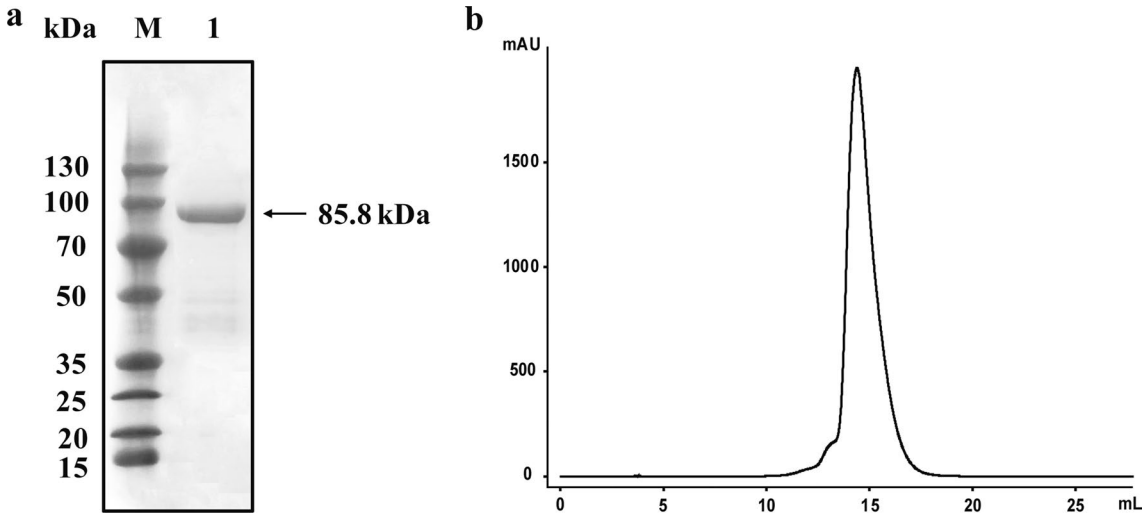

Fig. 2 Purification of the *Mf*Ago protein. **a** SDS-PAGE analysis of Ni–NTA-purified *Mf*Ago. M: protein marker; lane 1: purified *Mf*Ago. **b** Chromatograms of size-exclusion chromatography for *Mf*Ago. The measured UV absorbance (mAU) at 280 nm is shown against the elution volume (mL)

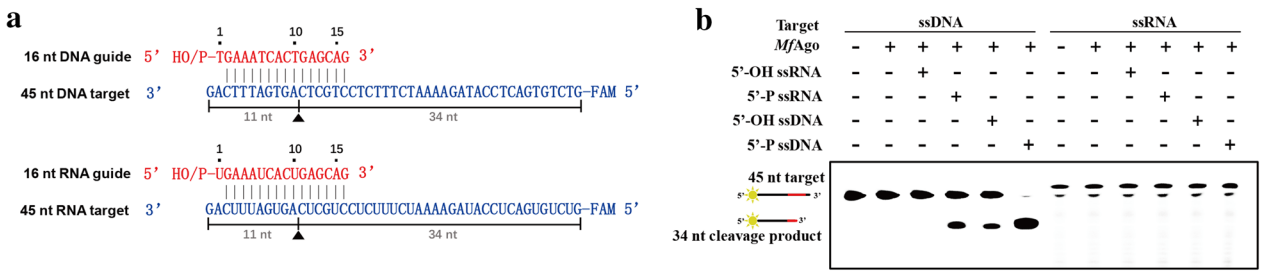

Fig. 3 Endonuclease activity assays of *Mf*Ago in vitro. **a** Synthetic DNA or RNA guides (red) and targets (blue). Predicted cleavage positions are indicated with a black triangle, black lines indicate the predicted 11- and 34-nt cleavage products. **b** Cleavage activity assay of *Mf*Ago with FAM-labeled DNA or RNA targets

Meanwhile, the results also indicated that, like other characterized Agos, *Mf*Ago cleaved the complementary target DNA strand at the complementary site between nucleotides 10 and 11 of the guide strand, but there were some differences in cleavage efficiency mediated by three different kinds of guides.

Mf Ago catalytic activity affected by temperature

The cleavage activity of active pAgos is strongly temperature dependent (Swarts et al. 2015a; Wang et al. 2009); thus, we tested the influence of temperature on recombinant *Mf*Ago ssDNA cleavage activity mediated by three different kinds of guides (Fig. 4). The optimum temperatures of *Mf*Ago were significantly different when directed by varied guides: the 5′-P ssDNA guide-mediated *Mf*Ago was most active in the range from 85 to 98.7 °C, achieving nearly 100% cleavage for the ssDNA target; the activity of 5′-OH ssDNA guide-mediated *Mf*Ago was enhanced with increasing temperature from 54.8 to 90 °C and then decreased rapidly with higher temperature (Fig. 4a), which might be caused by the weaker interaction between 5′-OH ssDNA guide and *Mf*Ago than interaction between 5′-P ssDNA guide and *Mf*Ago.

For the DNA cleavage of 5′-P ssRNA guide-mediated *Mf*Ago, we observed that the activity increased at the temperature range from 54.8 to 85 °C, then decreased rapidly at higher temperature and almost lost at 95 °C (Fig. 4b). Distinct to highly stable ssDNA guides, the 5′-P ssRNA guide could be degraded partially under high temperature (Additional file 1: Fig. S1). Therefore, we assumed that the reduction of *Mf*Ago cleavage activity over 85 °C might be a result of the 5′-P ssRNA degradation (Additional file 1: Fig. S2) together with the weakening interaction between guide and *Mf*Ago under high temperatures.

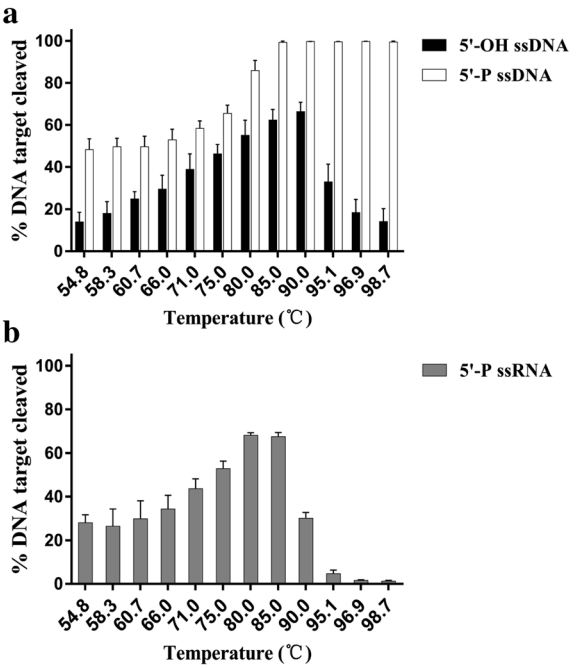

Fig. 4 Effect of temperature on *Mf*Ago activity. **a** Effect of temperature on *Mf*Ago activity mediated by 5′-P ssDNA and 5′-OH ssDNA guides. **b** Effect of temperature on *Mf*Ago activity mediated by 5′-P ssRNA guide. Error bars represent the SDs of three independent experiments

Mf Ago catalytic activity affected by divalent cations

Ago proteins are divalent cation-dependent endonucleases (Nowotny et al. 2005; Song et al. 2004), and the presence of divalent cations is essential for pAgos to specifically bind the 5′ end of the guide strand (Parker 2010; Sheng et al. 2014; Wang et al. 2009). To investigate which divalent cations *Mf*Ago can be utilized for cleavage, different divalent cations at a final concentration of 0.5 mM were added to the reaction system. *Mf*Ago was active

with Mn^{2+}, Co^{2+}, and Mg^{2+}, with Mn^{2+} giving higher activity than Co^{2+} and Mg^{2+} (Fig. 5a).

To further determine the optimal concentration of Mn^{2+} required for *Mf*Ago activity, a series of Mn^{2+} concentrations was used for *Mf*Ago activity analysis (Fig. 5b). Increased concentrations of Mn^{2+} improved *Mf*Ago activity mediated by three different guides. Interestingly, *Mf*Ago guide-mediated cleavage of ssDNA targets has different Mn^{2+} concentration requirements depending on the guide. *Mf*Ago that binds a 5′-P ssDNA guide cleaved almost 100% of ssDNA targets when the concentration of Mn^{2+} was greater than 10 μM. However, *Mf*Ago that binds 5′-OH ssDNA or 5′-P ssRNA guides cannot cleave the target nucleic acid completely, even at Mn^{2+} concentrations as high as 2000 μM.

Mf Ago catalytic activity strongly related to NaCl concentration

As NaCl plays an important role in maintaining the catalytic activity and stability of pAgos (Swarts et al. 2014a, 2015a), we investigated the effects of the NaCl concentration on *Mf*Ago activity (Fig. 6). *Mf*Ago activity mediated by the 5′-P ssDNA guide was highest in the NaCl concentration range from 100 to 1000 mM. *Mf*Ago activity mediated by 5′-P ssRNA and 5′-OH ssDNA guides achieves maximum cleavage at NaCl concentrations of 100 mM and 500 mM, respectively. Furthermore, higher NaCl concentrations could inhibit the cleavage activity of *Mf*Ago.

Kinetic performance of Mf Ago

To further investigate the catalytic properties of *Mf*Ago mediated by three different guides, we performed a cleavage kinetics assay at 85 °C with 250 mM NaCl and 2 mM Mn^{2+} (Fig. 7). The results indicated that *Mf*Ago exhibited the highest cleavage efficiency for the DNA target when utilizing the 5′-P ssDNA guide. In contrast, *Mf*Ago activity mediated by the 5′-OH ssDNA guide was less efficient, and the cleavage efficiency of *Mf*Ago using the 5′-P ssRNA guide was the lowest. Therefore, *Mf*Ago prefers to use 5′-P ssDNA nucleic acid as a guide strand.

Homology modeling and structural analysis of key interactions between guides and the MID domain of *Mf*Ago

Homology modeling has been extensively used to generate reliable three-dimensional protein structure models. With the complex structure of *Mj*Ago with its 5′-P ssDNA guide (PDB ID: 5G5T, identity 68%) as a template, we used SWISS-MODEL to construct the structure of *Mf*Ago (data not shown). Similarly, the architecture of

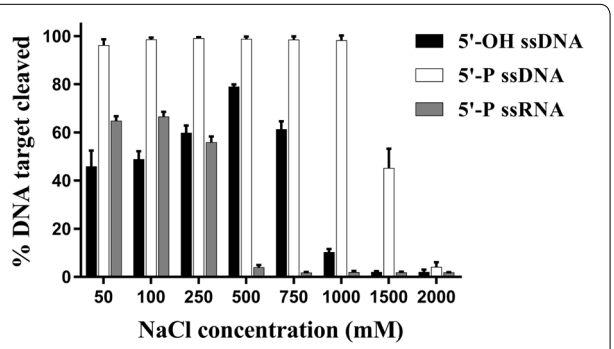

Fig. 6 Effect of NaCl on the enzyme activity of *Mf*Ago. Error bars represent the SDs of three independent experiments

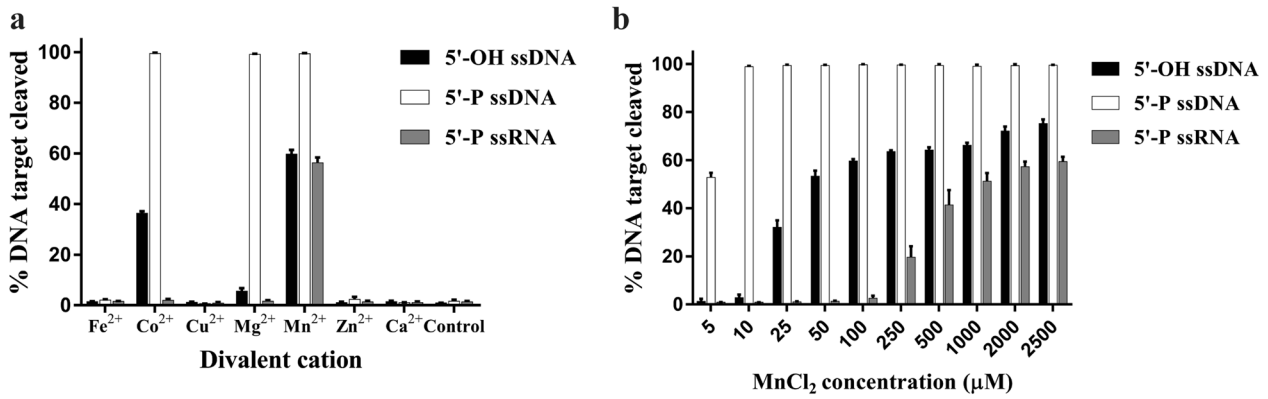

Fig. 5 Effects of different divalent cations and Mn^{2+} concentrations on *Mf*Ago activity. **a** Effect of different divalent cations on enzyme activity. **b** Effect of Mn^{2+} concentration on enzyme activity. Error bars represent the SDs of three independent experiments

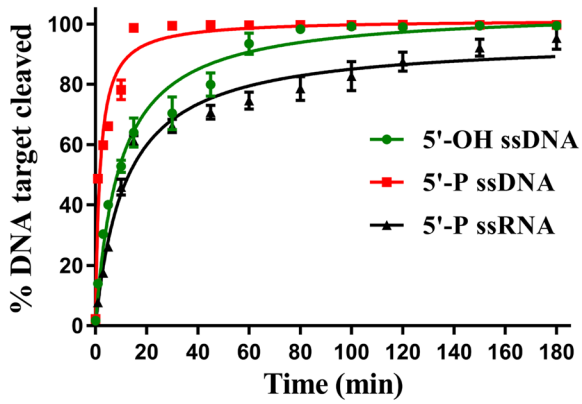

Fig. 7 Kinetic performance of *Mf*Ago mediated by three different kinds of guides. Assays were performed in three independent experiments and plotted using nonlinear regression. SDs are represented by error bars

*Mf*Ago displays a typical pAgo protein structure, which has four domains and two linker regions, forming a bilobal scaffold composed of a PIWI (P element-induced wimpy testis) domain, a MID (middle) domain, a PAZ (Piwi–Argonaute–Zwille) domain and an N-terminal domain, and connecting linkers L1 and L2 (Parker et al. 2005; Rashid et al. 2007; Schirle and MacRae 2012; Song et al. 2004).

To better understand the specific guide recognition mechanism of *Mf*Ago, the guides 5′-OH ssDNA, 5′-P ssDNA, and 5′-P ssRNA were individually docked into the *Mf*Ago structure. Ago proteins use a pocket in the MID domain for binding the 5′ end of guides (Kaya et al. 2016; Sheng et al. 2014); thus, potential interactions between the MID domain and different nucleic acid guides were examined (Fig. 8a–c). In previous studies, *Tt*Ago contains a binding pocket with multiple charged residues for recognizing and binding the 5′ phosphate group of the guide (Fig. 8d), while the MID-binding pocket of *Mp*Ago contains a hydrophobic pocket devoid of charged residues around the 5′-hydroxy group (Fig. 8e). In contrast, it seems that the MID-binding pocket of *Mf*Ago possesses both hydrophobic residues and hydrophilic residues and that the hydrophobic residues Leu^{453} and Tyr^{434} might interact with the 5′-hydroxyl group of guide DNA (Fig. 8a). Furthermore, the lack of a key α-helix that exists in *Mp*Ago at the C-terminus of the PIWI domain would result a less-compressed MID-binding pocket in *Mf*Ago, therefore providing sufficient space to bind the 5′ phosphate group.

Inspection of the structure of *Mf*Ago complexed with a 5′-OH ssDNA guide indicated that only residue Asp^{433} might form a single hydrogen bond with 5′-OH in ssDNA (Table 3). However, when the 5′-phosphate guide

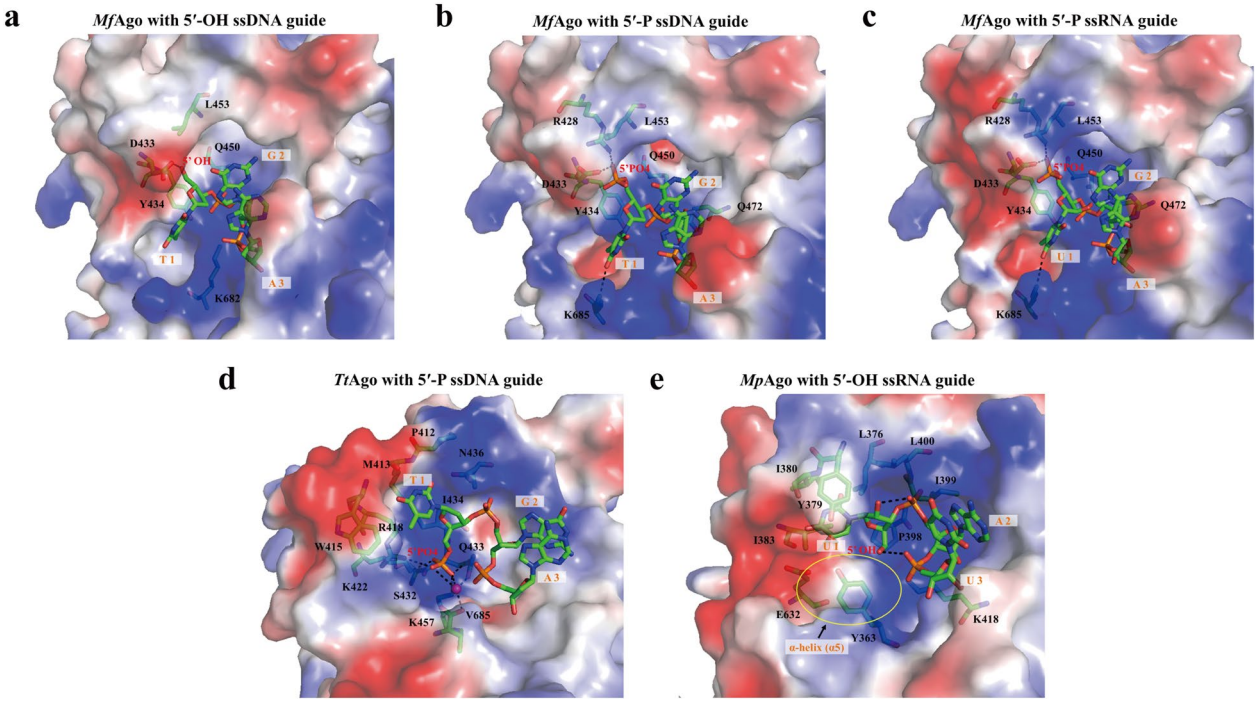

Fig. 8 The structural analysis and electrostatic heat map (red = negatively charged, blue = positively charged, white = neutral) of the binding pocket of *Mf*Ago for varied guides. The predicted binding pocket of *Mf*Ago with a 5′-OH ssDNA guide (**a**), 5′-P ssDNA guide (**b**), and 5′-P ssRNA guide (**c**). **d** The binding pocket of *Tt*Ago with a 5′-P ssDNA guide. **e** The binding pocket of *Mp*Ago with a 5′-OH ssRNA guide

Table 3 Residues of *Mf*Ago to interact with the 5′ end of the guide

Guide		*Mf*Ago		Distance (Å)
Type	Atom	Residue	Atom	
5′-OH ssDNA	O5′	Asp^{433}	$O^{\delta1}$	2.8
5′-P ssDNA	OP2	Arg^{428}	$N^{\eta1}$	2.9
	OP2	Asp^{433}	$O^{\delta1}$	2.5
	O4	Lys^{685}	N^{ζ}	3.3
5′-P ssRNA	OP2	Arg^{428}	$N^{\eta1}$	2.9
	OP2	Asp^{433}	$O^{\delta1}$	2.5
	O4	Lys^{685}	N^{ζ}	3.3

was docked into *Mf*Ago, the residues Arg^{428} and Asp^{433} in the MID domain created multiple hydrogen-bonding interactions with the phosphate group of the guide, and another key residue, Lys^{685}, is involved in hydrogen-bonding interactions with the 5′-terminal base of guide DNA/RNA, implying a stronger *Mf*Ago-binding affinity for 5′-P guides than for 5′-OH guides. These results might be the reason that the catalytic activity and optimal temperature of *Mf*Ago are higher with a 5′-P ssDNA guide than with a 5′-OH ssDNA guide.

Conclusion

*Mf*Ago was cloned and overexpressed in *E. coli* BL21(DE3). The biochemical characterization revealed that *Mf*Ago catalyzes ssDNA target cleavage directed by either 5′-P ssDNA, 5′-OH ssDNA, or 5′-P ssRNA guides, which is distinguished from the behavior of all other characterized eukaryotic or prokaryotic Agos. *Mf*Ago functions as an endonuclease for DNA target cleavage that requires divalent cations such as Mn^{2+}, Mg^{2+}, or Co^{2+} for its activity, with Mn^{2+} being the cation resulting in the highest activity. The maximum cleavage activity was achieved at 90 °C for 5′-OH ssDNA and 80–85 °C for 5′-P ssRNA guide-directed *Mf*Ago, whereas 85–98.7 °C was optimal for the 5′-P DNA guide-directed *Mf*Ago. Meanwhile, *Mf*Ago is quite active in reactions with an NaCl concentration less than 500 mM, whereas higher NaCl concentrations inhibit the activity of *Mf*Ago. Furthermore, our structural modeling studies revealed that *Mf*Ago has a distinct pocket in the MID domain for binding the 5′-end group of guides and that the different catalytic activities of *Mf*Ago with diverse guides might drive from varied hydrogen-binding interactions between the 5′-end group of guides and several key residues in this binding pocket. Characterization of *Mf*Ago expands the understanding of the pAgo family and will inspire the development of these new Ago proteins' potential applications in genetic manipulation.

Additional file

Additional file 1. Additional figures.

Abbreviations

Ago: argonaute protein; pAgo: prokaryotic argonaute protein; eAgo: eukaryotic argonaute protein; *Mf*Ago: *Methanocaldococcus fervens* argonaute protein; *Pf*Ago: *Pyrococcus furiosus* argonaute protein; *Aa*Ago: *Aquifex aeolicus* argonaute protein; *Mj*Ago: *Methanocaldococcus jannaschii* argonaute protein; *Tt*Ago: *Thermus thermophilus* argonaute protein; *Mp*Ago: *Marinitoga piezophila* argonaute protein; *Tp*Ago: *Thermotoga profunda* argonaute protein; *Rs*Ago: *Rhodobacter sphaeroides* argonaute protein; ssDNA: single-stranded DNA; 5′-P ssDNA: 5′-phosphorylated single-stranded DNA; 5′-OH ssDNA: 5′-hydroxylated single-stranded DNA; 5′-P ssRNA: 5′-phosphorylated single-stranded RNA; ARE: artificial restriction enzyme.

Acknowledgements

Not applicable.

Authors' contributions

YF conceived the study and modified the manuscript. YSC designed and performed the experiments, analyzed the data, and wrote the manuscript. QL was involved in project planning and manuscript revisions. FH constructed the *E. coli* BL21(DE3) expression vector and wrote a part of the manuscript. DS carried out the homology modeling and molecular docking. All authors read and approved the final manuscript.

Funding

This work was funded by the National Natural Science Foundation of China (31770078) and Ministry of Science and Technology (2017YFE0103300).

Availability of data and materials

All data generated or analyzed during this study are included in this published article.

Ethics approval and consent to participate

Not applicable.

Consent for publication

Not applicable.

Competing interests

The authors declare that they have no competing interests.

Received: 14 March 2019 Accepted: 16 May 2019
Published online: 05 June 2019

References

Bartel DP (2009) MicroRNAs: target recognition and regulatory functions. Cell 136(2):215–233. https://doi.org/10.1016/j.cell.2009.01.002

Doxzen KW, Doudna JA (2017) DNA recognition by an RNA-guided bacterial argonaute. PLoS ONE 12(5):e0177097. https://doi.org/10.1371/journal.pone.0177097

Enghiad B, Zhao H (2017) Programmable DNA-guided artificial restriction enzymes. ACS Synth Biol 6(5):752–757. https://doi.org/10.1021/acssynbio.6b00324

Kaya E, Doxzen KW, Knoll KR, Wilson RC, Strutt SC, Kranzusch PJ, Doudna JA (2016) A bacterial argonaute with noncanonical guide RNA specificity. Proc Natl Acad Sci USA 113(15):4057–4062. https://doi.org/10.1073/pnas.1524385113

Ketting RF (2011) The many faces of RNAi. Dev Cell 20(2):148–161. https://doi.org/10.1016/j.devcel.2011.01.012

Koonin EV (2017) Evolution of RNA- and DNA-guided antivirus defense systems in prokaryotes and eukaryotes: common ancestry vs convergence. Biol Direct 12(1):5. https://doi.org/10.1186/s13062-017-0177-2

Kumar S, Stecher G, Tamura K (2016) MEGA7: molecular evolutionary genetics analysis version 7.0 for bigger datasets. Mol Biol Evol 33(7):1870–1874. https://doi.org/10.1093/molbev/msw054

Makarova KS, Wolf YI, van der Oost J, Koonin EV (2009) Prokaryotic homologs of argonaute proteins are predicted to function as key components of a novel system of defense against mobile genetic elements. Biol Direct 4(1):29. https://doi.org/10.1186/1745-6150-4-29

Meister G (2013) Argonaute proteins: functional insights and emerging roles. Nat Rev Genet 14(7):447–459. https://doi.org/10.1038/nrg3462

Miyoshi T, Ito K, Murakami R, Uchiumi T (2016) Structural basis for the recognition of guide RNA and target DNA heteroduplex by argonaute. Nat Commun 7:11846. https://doi.org/10.1038/ncomms11846

Nowotny M, Gaidamakov SA, Crouch RJ, Yang W (2005) Crystal structures of RNase H bound to an RNA/DNA hybrid: substrate specificity and metal-dependent catalysis. Cell 121(7):1005–1016. https://doi.org/10.1016/j.cell.2005.04.024

Olovnikov I, Chan K, Sachidanandam R, Newman DK, Aravin AA (2013) Bacterial argonaute samples the transcriptome to identify foreign DNA. Mol Cell 51(5):594–605. https://doi.org/10.1016/j.molcel.2013.08.014

Parker JS (2010) How to slice: snapshots of argonaute in action. Silence 1(1):3. https://doi.org/10.1186/1758-907X-1-3

Parker JS, Roe SM, Barford D (2005) Structural insights into mRNA recognition from a PIWI domain–siRNA guide complex. Nature 434(7033):663–666. https://doi.org/10.1038/nature03462

Rashid UJ, Paterok D, Koglin A, Gohlke H, Piehler J, Chen JC (2007) Structure of *Aquifex aeolicus* argonaute highlights conformational flexibility of the PAZ domain as a potential regulator of RNA-induced silencing complex function. J Biol Chem 282(18):13824–13832. https://doi.org/10.1074/jbc.M608619200

Repasky MP, Shelley M, Friesner RA (2007) Flexible ligand docking with glide. Curr Protoc Bioinform. https://doi.org/10.1002/0471250953.bi0812s18

Rivas FV, Tolia NH, Song JJ, Aragon JP, Liu J, Hannon GJ, Joshua-Tor L (2005) Purified argonaute2 and an siRNA form recombinant human RISC. Nat Struct Mol Biol 12(4):340–349. https://doi.org/10.1038/nsmb918

Robert X, Gouet P (2014) Deciphering key features in protein structures with the new ENDscript server. Nucleic Acids Res 42:W320–W324. https://doi.org/10.1093/nar/gku316

Ryazansky S, Kulbachinskiy A, Aravin AA (2018) The expanded universe of prokaryotic argonaute proteins. Mbio. https://doi.org/10.1128/mBio.01935-18

Schirle NT, MacRae IJ (2012) The crystal structure of human argonaute2. Science 336(6084):1037–1040. https://doi.org/10.1126/science.1221551

Sheng G, Zhao H, Wang J, Rao Y, Tian W, Swarts DC, van der Oost J, Patel DJ, Wang Y (2014) Structure-based cleavage mechanism of *Thermus thermophilus* argonaute DNA guide strand-mediated DNA target cleavage. Proc Natl Acad Sci USA 111(2):652–657. https://doi.org/10.1073/pnas.1321032111

Siomi MC, Sato K, Pezic D, Aravin AA (2011) PIWI-interacting small RNAs: the vanguard of genome defence. Nat Rev Mol Cell Biol 12(4):246–258. https://doi.org/10.1038/nrm3089

Song JJ, Smith SK, Hannon GJ, Joshua-Tor L (2004) Crystal structure of argonaute and its implications for RISC slicer activity. Science 305(5689):1434–1437. https://doi.org/10.1126/science.1102514

Swarts DC, Jore MM, Westra ER, Zhu Y, Janssen JH, Snijders AP, Wang Y, Patel DJ, Berenguer J, Brouns SJJ, van der Oost J (2014a) DNA-guided DNA interference by a prokaryotic argonaute. Nature 507(7491):258–261. https://doi.org/10.1038/nature12971

Swarts DC, Makarova K, Wang Y, Nakanishi K, Ketting RF, Koonin EV, Patel DJ, van der Oost J (2014b) The evolutionary journey of argonaute proteins. Nat Struct Mol Biol 21(9):743–753. https://doi.org/10.1038/nsmb.2879

Swarts DC, Hegge JW, Hinojo I, Shiimori M, Ellis MA, Dumrongkulraksa J, Terns RM, Terns MP, van der Oost J (2015a) Argonaute of the archae on *Pyrococcus furiosus* is a DNA-guided nuclease that targets cognate DNA. Nucleic Acids Res 43(10):5120–5129. https://doi.org/10.1093/nar/gkv415

Swarts DC, Koehorst JJ, Westra ER, Schaap PJ, van der Oost J (2015b) Effects of argonaute on gene expression in *Thermus thermophilus*. PLoS ONE 10(4):e0124880. https://doi.org/10.1371/journal.pone.0124880

Swarts DC, Szczepaniak M, Sheng G, Chandradoss SD, Zhu Y, Timmers EM, Zhang Y, Zhao H, Lou J, Wang Y, Joo C, van der Oost J (2017) Autonomous generation and loading of DNA guides by bacterial argonaute. Mol Cell 65(6):985–998. https://doi.org/10.1016/j.molcel.2017.01.033

Thompson JD, Higgins DG, Gibson TJ (1994) CLUSTAL W: improving the sensitivity of progressive multiple sequence alignment through sequence weighting, position-specific gap penalties and weight matrix choice. Nucleic Acids Res 22(22):4673–4680

Wang Y, Juranek S, Li H, Sheng G, Tuschl T, Patel DJ (2008a) Structure of an argonaute silencing complex with a seed-containing guide DNA and target RNA duplex. Nature 456(7224):921–926. https://doi.org/10.1038/nature07666

Wang Y, Sheng G, Juranek S, Tuschl T, Patel DJ (2008b) Structure of the guide-strand-containing argonaute silencing complex. Nature 456(7219):209–213. https://doi.org/10.1038/nature07315

Wang Y, Juranek S, Li H, Sheng G, Wardle GS, Tuschl T, Patel DJ (2009) Nucleation, propagation and cleavage of target RNAs in Ago silencing complexes. Nature 461(7265):754–761. https://doi.org/10.1038/nature08434

Waterhouse A, Bertoni M, Bienert S, Studer G, Tauriello G, Gumienny R, Heer FT, de Beer TAP, Rempfer C, Bordoli L, Lepore R, Schwede T (2018) SWISS-MODEL: homology modelling of protein structures and complexes. Nucleic Acids Res 46(W1):W296–W303. https://doi.org/10.1093/nar/gky427

Willkomm S, Oellig CA, Zander A, Restle T, Keegan R, Grohmann D, Schneider S (2017) Structural and mechanistic insights into an archaeal DNA-guided argonaute protein. Nat Microbiol 2:17035. https://doi.org/10.1038/nmicrobiol.2017.35

Yuan YR, Pei Y, Ma JB, Kuryavyi V, Zhadina M, Meister G, Chen HY, Dauter Z, Tuschl T, Patel DJ (2005) Crystal structure of *A. aeolicus* argonaute, a site-specific DNA-guided endoribonuclease, provides insights into RISC-mediated mRNA cleavage. Mol Cell 19(3):405–419. https://doi.org/10.1016/j.molcel.2005.07.011

Yuan YR, Pei Y, Chen HY, Tuschl T, Patel DJ (2006) A potential protein-RNA recognition event along the RISC-loading pathway from the structure of *A. aeolicus* argonaute with externally bound siRNA. Structure 14(10):1557–1565. https://doi.org/10.1016/j.str.2006.08.009

Zander A, Holzmeister P, Klose D, Tinnefeld P, Grohmann D (2014) Single-molecule FRET supports the two-state model of argonaute action. RNA Biol 11(1):45–56. https://doi.org/10.4161/rna.27446

Zander A, Willkomm S, Ofer S, van Wolferen M, Egert L, Buchmeier S, Stöckl S, Tinnefeld P, Schneider S, Klingl A, Albers SV, Werner F, Grohmann D (2017) Guide-independent DNA cleavage by archaeal argonaute from *Methanocaldococcus jannaschii*. Nat Microbiol 2:17034. https://doi.org/10.1038/nmicrobiol.2017.34

Publisher's Note